Applied Catalysis B: Environmental 179 (2015) 439–444

Contents lists available at ScienceDirect

Applied Catalysis B: Environmental

journal homepage: www.elsevier.com/locate/apcatb

Nickel-based anode with microstructured molybdenum dioxide internal reformer for liquid hydrocarbon-fueled solid oxide fuel cells

Byeong Wan Kwon[a,c], Shuozhen Hu[a], Qian He[b], Oscar G. Marin-Flores[b], Chang Hoon Oh[c], Sung Pil Yoon[c], Jinsoo Kim[d], Joe Breit[e], Louis Scudiero[f], M. Grant Norton[b], Su Ha[a,d,*]

[a] Voiland School of Chemical Engineering and Bioengineering, Washington State University, P.O. Box 642710, Pullman, WA 99164-2710, USA
[b] School of Mechanical and Materials Engineering, Washington State University P.O. Box 642920, Pullman, WA 99164-2920, USA
[c] Fuel Cell Research Center, Korea Institute of Science and Technology, Hwarang-ro 14-gil, Seongbuk-gu, Seoul 136-791, Republic of Korea
[d] Department of Chemical Engineering, Kyung Hee University, Yongin, Kyunggi-do 449-701, Republic of Korea
[e] System Concept Center, Boeing Commercial Airplanes, 6600 Merrill Creek Pkwy., Everett, WA 98203, USA
[f] Chemistry Department and Materials Science and Engineering Program, Washington State University, Pullman, WA 99164, USA

ARTICLE INFO

Article history:
Received 23 February 2015
Received in revised form 16 May 2015
Accepted 22 May 2015
Available online 27 May 2015

Keywords:
Internal micro-reformer
Solid oxide fuel cells
Molybdenum dioxide
n-dodecane
O_2/C ratio

ABSTRACT

The present paper describes the fabrication of a bilayer structured solid oxide fuel cell (SOFC). Its anode consists of molybdenum dioxide (MoO_2)-based internal micro-reformer in the form of a porous thin film deposited over conventional Ni/YSZ cermet. Cell performance was measured by directly feeding a mixture of *n*-dodecane and air at different O_2/C ratios to the anode at 750 °C. Our findings show that the bilayer structured SOFC operating at an O_2/C ratio of 0.64 led to the highest initial cell performance with an initial maximum power density >4.0 W cm^{-2}. At a constant voltage of 0.7 V and O_2/C ratio of 0.64, the bilayer structured SOFC showed a gradual increase in power density output over the first 2 h, followed by a stable output of 3.6 W cm^{-2} for the next 10 h. The tested cell showed no indication of coking and phase transformation. When a conventional Ni-based SOFC without the internal micro-reformer was operated under similar conditions, its initial performance and long-term stability were found to be significantly lower than that of bilayer structured SOFC due to Ni oxidation under high O_2/C ratio or coking under the low O_2/C ratio. These results open up new opportunities for efficiently generating electrical power from various types of high energy density liquid fuels using SOFCs with an integrated MoO_2 micro- reformer.

1. Introduction

Solid oxide fuel cells (SOFCs) are a promising technology because they can efficiently and directly convert the chemical energy of fuels into electrical energy [1–3]. Due to the high operating temperatures (typically 600–1000 °C), SOFCs hold particular promise because of their ability to use a variety of complex liquid fuels, such as conventional liquid transportation fuels (e.g., gasoline, diesel-like fuels and jet fuels) and next generation liquid bio-fuels (e.g., biodiesel), either by using external reforming systems or directly feeding these fuels into their inexpensive transition metal-based anodes [4,5].

Nickel (Ni)-based anodes are commonly used in SOFCs owing to their low cost, good chemical stability, and excellent catalytic activity toward hydrogen oxidation and reforming of small hydrocarbon molecules. However, Ni-based anodes are well known for promoting severe surface carbon deposition. Excessive formation of carbon deposits on the anode leads to a rapid deterioration of the cell performance by physically blocking access of the reactants to the active catalyst sites [6–11]. To operate Ni-based SOFCs by directly feeding liquid hydrocarbon fuels, a thin catalytic layer can be deposited over the Ni-based anode to act as an internal micro-reformer. In previous work conducted by Zhan and Barnett, a ruthenium oxide-based internal micro-reformer was used to directly operate a SOFC with complex liquid fuels at the O_2/C ratios ranging from 0.66 to 0.88 [12]. However, ruthenium oxide is expensive and its use would significantly increase the overall cost of SOFCs. Thus, an alternative and inexpensive catalytic material with high reforming activity and good stability toward complex liquid fuels is required to fabricate the internal micro-reformer over a Ni-based anode.

* Corresponding author at: Voiland School of Chemical Engineering and Bioengineering, Washington State University, P.O. Box 642710, Pullman, WA 99164-2710, USA. Tel.: +1 509 335 3786; fax : +1 509 335 4806.
E-mail address: suha@wsu.edu (S. Ha).

http://dx.doi.org/10.1016/j.apcatb.2015.05.048
0926-3373/

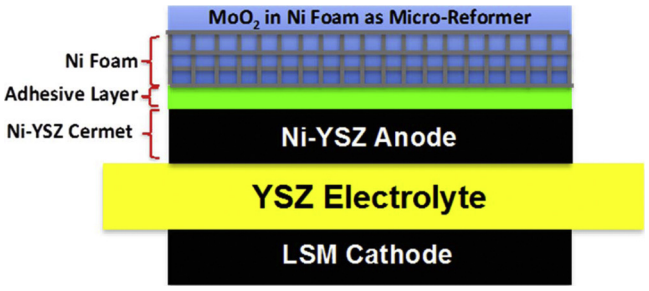

Fig. 1. Schematic of Ni-based SOFC with an internal MoO_2 micro-reformer layer.

In previous work, we successfully synthesized nanoparticle molybdenum dioxide (MoO_2) that displays not only high reforming activity for various liquid hydrocarbons but also excellent coking tolerance [13,14]. The catalytic activity has been explained in terms of a reaction mechanism similar to that proposed by Mars and van Krevelen [13]. The capability of MoO_2 to selectively transfer lattice oxygen to hydrocarbon molecules is believed to reduce the amount of carbon accumulated on the catalyst surface, thus minimizing coke formation during the reformation of logistics fuels [13,15,16]. In addition, MoO_2 possesses a significant metallic component to its interatomic bonding and displays metallic-like electronic conductivity comparable to that of highly conductive oxides such as ReO_3, as a result of a relatively high density of states in the valence band [17–19].

In the present paper, we describe the fabrication and performance of MoO_2-based internal micro-reformer, which consists of a porous thin film deposited over the conventional Ni-based anode. The results of operating the cell with *n*-dodecane are compared with a conventional Ni-based SOFC without internal micro-reformer. The tested cells are characterized using various analytical techniques including scanning electron microscopy (SEM) with energy dispersive X-ray analysis (EDX), X-ray diffraction (XRD), and X-ray photoelectron spectroscopy (XPS).

2. Experimental

The anode of our bilayer structured SOFC consisted of three major components: the Ni-YSZ cermet, an adhesive layer, and the MoO_2-covered Ni foam, as shown in Fig. 1. The Ni foam with a thickness of 0.72 mm was mechanically cut into a $1 \times 1\ cm^2$ square shape. A slurry was prepared to serve as an adhesive layer, which allows one to physically attach the Ni foam over the Ni-YSZ cermet. The composition of the slurry was 3 wt.% binder (Butvar B-98; Sigma–Aldrich, St. Louis, MO), 5 wt.% dispersant (polyvinylpyrrolidone; Sigma–Aldrich, St. Louis, MO), 3 wt.% pore former (polyvinyl alcohol; Sigma–Aldrich, St. Louis, MO), 50 wt.% solvent (isopropyl alcohol; Sigma–Aldrich, St. Louis, MO), and appropriate amounts of NiO and YSZ powders. All the components were physically mixed to form the adhesive slurry. A commercial half-cell consisting of a Ni-YSZ cermet (anode) and YSZ electrolyte (Fuel Cell Materials, Lewis Center, OH) was used to fabricate the bilayer structure SOFC. The thicknesses of the YSZ electrolyte and the Ni-based anode for the commercial half-cell were 150 μm and 50 μm, respectively. The electrode diameter was 12.5 mm, while that of the electrolyte was 25 mm.

The adhesive slurry and Ni-foam were applied to the Ni-YSZ cermet of the half-cell and calcined at 900 °C for 2 h in static air to burn out the organic compounds. Subsequently, the calcined body was sintered at 1400 °C for 10 h to achieve good adhesion between the different layers [20]. Without the Ni foam, the MoO_2 in the micro-reformer layer oxidizes to the inactive MoO_3 phase by reacting with lattice oxygen from the YSZ electrolyte during the cell operation. Since the Ni foam cannot conduct oxygen ions, it acts as a protective layer to prevent the MoO_2 reforming layer from oxidizing. Sr-doped $LaMnO_3$ (LSM) (Fuel Cell Materials, Lewis Center, OH) and an organic binder (V-006A; Heraeus, W. Conshohocken, PA) were mixed in a ratio of 60:40 (by weight) to prepare a slurry, which was painted as the cathode on the YSZ electrolyte surface of the half-cell followed by drying at 120 °C. The cathode was further sintered at 1100 °C for 2 h in air. Before preparing the internal MoO_2 micro-reformer, the Ni-based anode was completely reduced in flowing H_2 at 850 °C for 7 h.

Once the Ni foam was incorporated into the button cell, a nanoparticle MoO_2 catalyst ink was electrosprayed over the Ni foam [21]. To obtain the MoO_2 thin film with the necessary pore structure and morphology, the deposition parameters were kept at the following values: substrate temperature at 300 °C; flow rate of suspension at $2\ mL\ h^{-1}$; nozzle-to- substrate distance of 6 cm; applied voltage at 10 kV; deposition time for 1 h. During electrospraying, the MoO_2 nanoparticles filled and eventually covered the Ni foam. Subsequently, an additional layer of MoO_2 catalyst ink was painted on the surface of the MoO_2-filled Ni foam. This catalyst ink was prepared by mixing commercial MoO_2 particles (Alfa Aesar, Ward Hill, MA) with a solution of nanopure water and polyvinyl alcohol [22].

The cell testing system used in this work consisted of two concentric quartz tubes with two furnaces. The fuel mixture was introduced through the inner tube, while the outer tube served as an exhaust line. The lower furnace was used to vaporize the fuel at 350 °C, whereas the upper furnace was used to heat the cell to 750 °C. Air was used as the oxygen source for the cathode and was allowed to flow through the insulation on the upper furnace into the cathode via natural convection. The fuel mixture that was directly fed to the anode consisted of mixtures of *n*-dodecane and air at oxygen- to-carbon molar ratios (O_2/C) of 0.60, 0.64, and 0.70. The flow rate of *n*-dodecane was maintained at $0.3\ mL\ h^{-1}$. Based on our previous works, the range of O_2/C ratios used for this study was determined to prevent an undesired phase transformation of MoO_2 into either Mo_2C or MoO_3 [13–16]. If the O_2/C ratio is lower than this range at 750 °C, MoO_2 would reduce to Mo_2C and eventually lead to the severe carbon deposition. On the other hand, if the O_2/C ratio is higher than this range at 750 °C, MoO_2 would oxidize to inactive MoO_3. After operating Ni-based SOFCs with and without the MoO_2 internal micro-reformer, the tested anode layers were analyzed to determine the degree of coke formation using SEM (FEI Sirion operated at 15 kV) with EDX, XRD (Philips diffractometer using Co Kα radiation with an Fe filter), and XPS (AXIS-165 using achromatic MgKα (1254 eV) X-ray radiation with a power of 210 W). For these measurements, we used a blade to carefully remove the tested anode layers from the electrolyte surface. For the bilayer structured SOFC operating at the O_2/C ratio of 0.64, we could separate the MoO_2-based internal micro-reformer layer from the Ni-based electrode layer. Thus, we crushed each layer into the power form without mixing them up for the measurements.

3. Results and discussion

Fig. 2 shows initial cell voltage and power density as a function of the current density for the bilayer structured SOFCs operated at 750 °C using O_2/C ratios of 0.60, 0.64, and 0.70. According to Fig. 2, the initial OCV of the bilayer structured SOFC decreases from 1.065 to 0.944 V as the O_2/C ratio increases from 0.60 to 0.70. As the mixture of *n*-dodecane and air is directly fed into the bilayer structured anode, syngas is being produced through the partial oxidation process. However, as the O_2/C ratio increases, full oxidation of the fuel becomes dominant and the amount of syngas decreases. As the reforming gas stream with a lower concentration of syngas (i.e.,

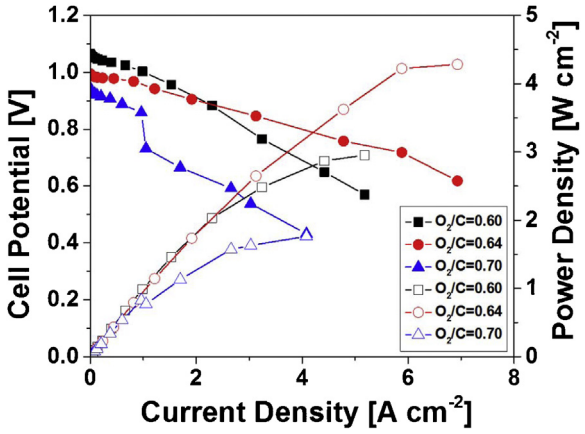

Fig. 2. Initial cell potential and power density vs. current density plots for the bilayer structured SOFC using the *n*-dodecane and air mixtures with the different O_2/C ratios at 750 °C. The closed symbols are used for the cell potential vs. current density plots, and the open symbols are used for the power density vs. current density plots.

higher concentration of CO_2 and H_2O) diffuses into the Ni-based anode from the MoO_2 micro-reformer layer, the initial OCV of the bilayer structured SOFC decreases in accordance with the Nernst equation.

Unlike the initial OCV value, the initial power density output increases as the O_2/C ratio increases from 0.60 to 0.64 followed by a decrease as the O_2/C ratio further increases from 0.64 to 0.70. At the O_2/C ratio of 0.60, the MoO_2 phase was transformed into the Mo_2C phase, which leads to the mixed phase (XRD data not shown). For the partial oxidation reaction of complex liquid fuels like *n*-dodecane, we have observed that its reforming performance in terms of H_2 and CO yields are lower over the mixed phase compared to that of the pure MoO_2 phase [18]. As the O_2/C ratio increases from 0.60 to 0.64, the transformation of the MoO_2 phase into the Mo_2C phase and the formation of this mixed phase were prevented (XRD data shown in Fig. 3) [13], which leads to the higher initial reforming and cell performances. However, at the O_2/C ratio of 0.70, there is enough oxygen to oxidize (i) MoO_2 to MoO_3 in the micro-reformer layer and (ii) Ni to NiO in the Ni-based anode layer. These bulk phase oxidations are observed in the XRD pattern of the tested cells (XRD data not shown). In summary, the maximum initial power density output of 4.3 W cm^{-2} at 0.6 V occurs for the bilayer structured SOFC operating at the O_2/C ratio of 0.64, which seems to be the optimum ratio.

Fig. 4 shows a plot of the power density at a constant voltage of 0.7 V versus time for the bilayer structured SOFC operating at the optimum O_2/C ratio of 0.64. As seen, the power density output gradually increases for the first 2 h and becomes stable at ~3.6 W cm^{-2} for the following 8 h of testing. After operating the cell for the first 10 h, the power density output at 0.7 V starts to decrease from ~3.6 W cm^{-2} to ~2.5 W cm^{-2} over the operation time of 2 h and maintains this power density output for the remainder of the test. It is important to point out that, over the entire 24 h testing of the cell at the O_2/C ratio of 0.64, no pressure drop was noticed, which is a good indication of no coking.

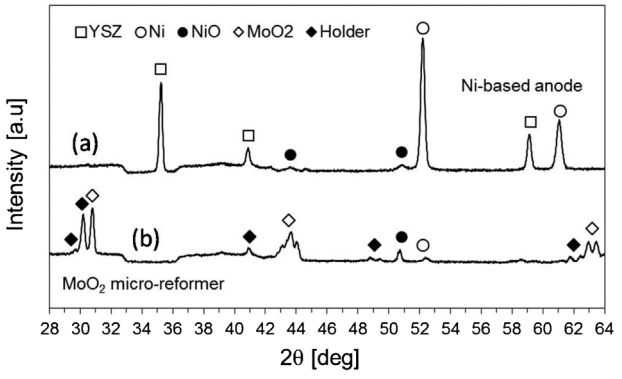

Fig. 3. XRD patterm of (a) MoO_2 micro-reformer and (b) Ni-based anode layers obtained from the bilayer structured SOFC after operating for 24 h using the *n*-dodecane/air mixture as fuel at the O_2/C ratio of 0.64 and 750 °C.

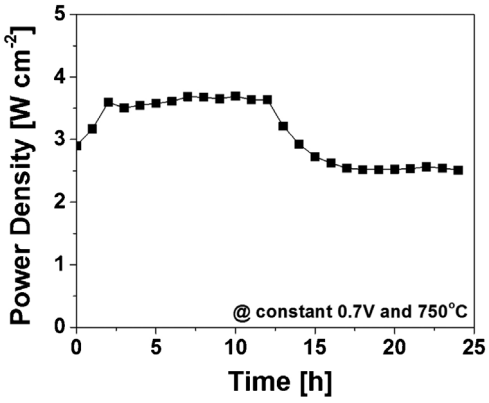

Fig. 4. Power density vs. time at the constant voltage of 0.7 V for the bilayer structured SOFC using the *n*-dodecane and air mixture with the O_2/C ratios of 0.64 at 750 °C.

After operating the bilayer structured SOFC for 24 h at the O_2/C ratio of 0.64, the MoO_2 micro-reformer and Ni-based anode layers were carefully separated into two individual layers from the YSZ electrolyte surface. Fig. 4 shows the XRD pattern of these two individual layers (i.e., the tested MoO_2 micro-reformer and the Ni-based anode layers). For the XRD pattern of the tested MoO_2 micro-reformer layer, the peaks at $2\theta = 30.8°$, 43.5°, and 63.2° are attributed to the monoclinic structure of MoO_2. The peaks at $2\theta = 40.60°$, 44.80° and 46.60° that are commonly assigned to the carbide phase were not observed. Also, no diffraction peaks from the MoO_3 phase were observed. Furthermore, no broad diffraction peak was detected at $2\theta = 30.5°$, which suggests either an absent or negligible coke formation [23]. The diffraction pattern of the tested Ni-based anode shows a very small diffraction peak at $2\theta = 50.8°$, which indicates that a very small amount of metallic Ni oxidized to form the NiO phase over the 24 h test. Thus, this finding shows that the O_2/C ratio of 0.64 was not able to significantly oxidize the Ni-based anode in the bilayer structured SOFC since most of the O_2 is being consumed by the MoO_2 micro-reformer layer through the partial oxidation of the fuel. The tested Ni-based anode also shows no presence of coking. To summarize, XRD analysis of both the MoO_2 micro-reformer and Ni-based anode layers indicate that (i) the O_2/C ratio of 0.64 is high enough to prevent the bulk reduction of MoO_2 to the carbide phase as well as coking and (ii) the same ratio is also low enough to prevent any significant bulk oxidation of Ni to NiO and MoO_2 to MoO_3.

In order to further prove that the O_2/C ratio of 0.64 prevents coke formation over the bilayer structured anode, SEM-EDX and XPS analysis were performed on the tested cell after operating it for 24 h. For the analysis, both the MoO_2 micro-reformer and Ni-based anode layer were carefully detached from the YSZ electrolyte as two individual layers. Fig. 5 shows the EDX spectra observed from multiple point analyses and the carbon 1s XPS spectra of the tested MoO_2 micro-reformer and Ni-based anode layers. According to EDX, the tested bilayer structured SOFC does not contain any detectible elemental carbon. The carbon 1 s XPS spectrum of the tested MoO_2 micro- reformer layer shows no peak associated with graphitic carbon, whereas the Ni anode layer displays a small peak at a BE of 284.6 eV, which is attributed to the presence of elemental

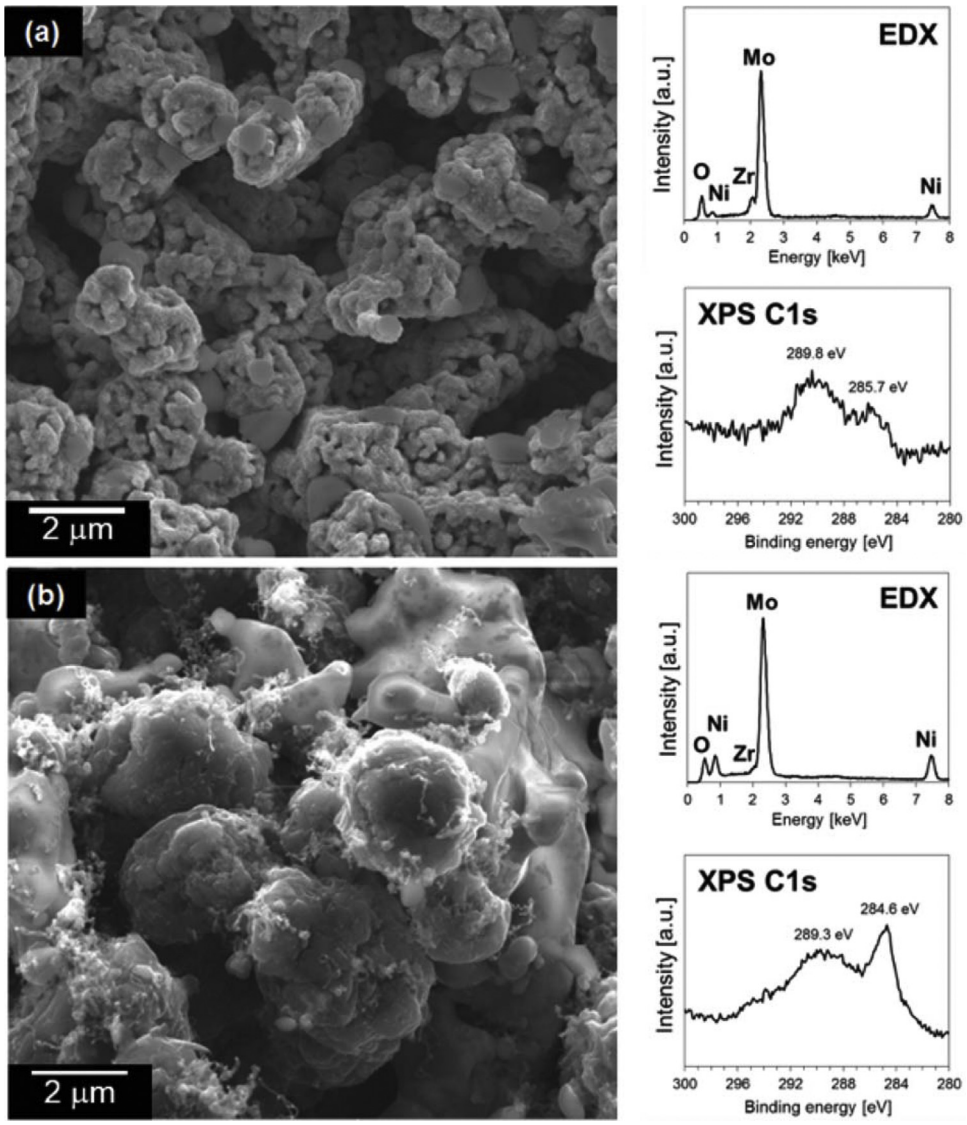

Fig. 5. SEM-EDX analysis and XPS spectra of (a) MoO_2 micro- reformer and (b) Ni-based anode layers obtained from the bilayer structured SOFC after operating it for 24 h using the *n*-dodecane/air mixture as fuel at the O_2/C ratio of 0.64 and 750 °C.

carbon. However, the intensity of this peak is much lower than that observed on the coked sample after operating the cell at the O_2/C ratio of 0.60 (not shown in Figure). Thus, SEM-EDX and XPS analysis support the fact that the tested bilayer structured SOFC operating at the O_2/C ratio of 0.64 over 24 h forms negligible amounts of coke. Thus, the power density drop observed in the bilayer structured SOFC after operating the cell at the constant voltage of 0.7 V and the O_2/C ratio of 0.64 for the first 10 h (see Fig. 4) is due to neither the phase transformation of the active MoO_2 layers nor surface coking. One possible explanation for this performance drop could be a decrease of MoO_2 surface area for the internal reforming layer due to sintering over the operation time. Comparing to Ni nanoparticles, MoO_2 nanoparticles are much harder to sinter. Nevertheless, MoO_2 nanoparticles in the internal reforming layer would still sinter slowly over the operation time. It seems that the overall cell performance is not limited by the number of MoO_2 active site for the first 10 h. However, it would become the limiting factor for the overall cell performance beyond the operation time of 10 h as its surface area decreases down to some critical value**.** As a part of our future work, we will investigate the reason for this power density drop in detail as well as the cell performance beyond 24 h using the O_2/C ratio of 0.64.

The cell performances between the bilayer structured SOFC and the conventional Ni-based SOFC were also compared. Thus, Fig. 6(a) shows the power density at a constant cell voltage of 0.7 V versus time for (i) the bilayer structured SOFC at the O_2/C ratio of 0.64 and (ii) the Ni-based SOFCs at two different O_2/C ratios, 0.60 and 0.20. For the Ni-based SOFC tested at the O_2/C ratio of 0.60, the power density at the constant voltage of 0.7 V starts at a much lower value of 0.045 W cm^{-2} and remains the same for the entire 10 h test. We also plotted their initial cell voltage and power density as a function of the current density (not shown in figure), which indicates the superior initial performances of the bilayer structured SOFC over the Ni-based conventional SOFC. Overall, the power density output of the bilayer structured SOFC at the O_2/C ratio of 0.64 is much higher than that of the Ni-based SOFC at the O_2/C ratio of 0.60 over their 24 h tests. Fig. 6(b) shows the XRD pattern of the anode collected from the conventional Ni-based SOFC after its 10 h operation at the O_2/C ratio of 0.60. Before the XRD measurement, the Ni-based anode was carefully detached from the YSZ electrolyte. Its XRD pattern displays the high intensity peaks for both the Ni and NiO phases, which indicates that the O_2/C ratio of 0.60 at 750 °C is high enough to promote oxidation of Ni to NiO. In the case of the bilayer structured SOFC, the MoO_2 micro-reformer layer first

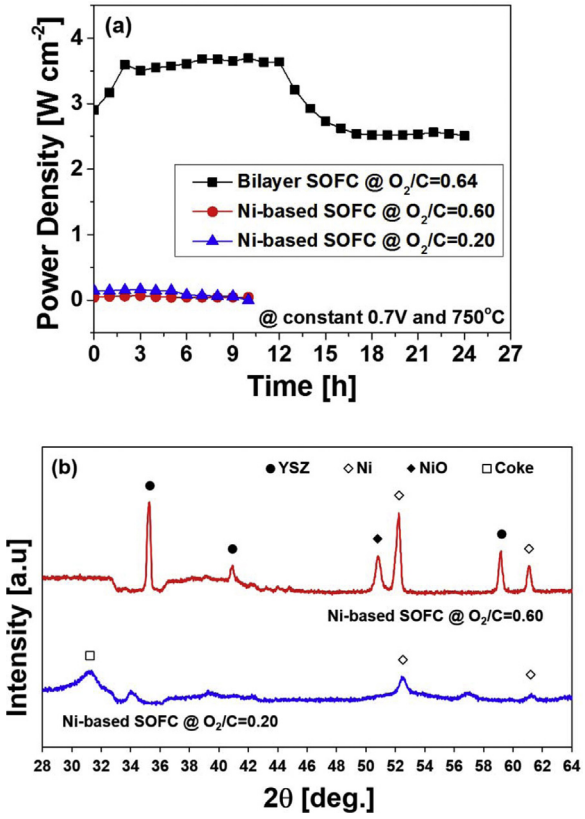

Fig. 6. (a) Power density at the constant voltage of 0.7 V vs. time for the bilayer structured SOFC and Ni-based SOFCs using the *n*-dodecane fuel mixtures at different O_2/C ratios and 750 °C, (b) XRD pattern of the Ni-based SOFC after operating it for 10 h.

consumes oxygen via the partial oxidation reaction of *n*-dodecane before it reaches the Ni-based anode. Consequently, the Ni-based anode of the bilayer structured SOFC only interacts with the reforming gas product at a significantly lower oxygen partial pressure, thus preventing the oxidation of its Ni-based anode (see Fig. 3). Hence, the bilayer structured SOFC shows the higher initial power density output at the constant voltage of 0.7 V as shown in Fig. 6(a). Since the Ni-based conventional SOFC would be completely oxidized to form the NiO phase and produce zero powers under the O_2/C ratio of 0.64, its performance is not tested at such high O_2/C ratio.

The initial impedance spectra of the bilayer structured SOFC and the Ni-based SOFCs are also measured as shown in Fig. 7. The ionic resistance of the cells was determined from the high-

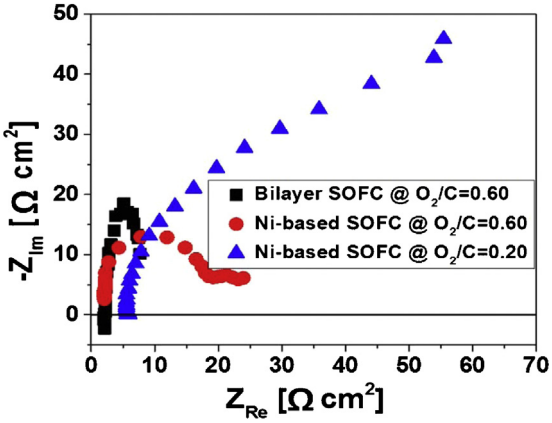

Fig. 7. Impedance spectra of the bilayer structured SOFC and Ni-based SOFC operating with the *n*-dodecane fuel mixtures using different O_2/C ratios at 750 °C.

frequency intercept with the abscissa in the impedance plots. The charge transfer resistances can also be estimated by measuring the radius of the hemi-circles shown in the impedance plots. Using the considerations mentioned above, the electrolyte resistances (R_{ele}) of both SOFCs with and without the micro-reformer layer at the O_2/C ratio of 0.60 were found to be 2.20 Ω cm^2, which suggests that the presence of the MoO_2 micro-reformer on the Ni-based anode does not affect the overall ionic conductivity of the Ni-based SOFC. This result also indicates that our bilayer structured SOFC design effectively prevents the ion flux between the MoO_2 micro-reformer and YSZ electrolyte membrane layers. At the O_2/C ratio of 0.60, the charge transfer resistance ($R_{anode,ct}$) of the bilayer SOFCs was found to be 6.25 Ω cm^2, while that of the Ni-based SOFCs was estimated as 24.21 Ω cm^2. The impedance of the bilayer structured SOFC is about a factor of four lower than that of the Ni-based SOFC at the selected O_2/C ratio. Thus, the impedance data agree well with the cell performance data shown in Fig. 6(a) as the bilayer structured SOFC with the lower charge transfer resistance shows a much higher initial cell performance than the Ni-based SOFC with the higher charge transfer resistance. Based on these initial impedance and cell performance data, we speculate that Ni oxidation under the O_2/C ratio of 0.60 occurs during the initial cell operation time (almost immediately). Thus, oxidation of the Ni-based SOFC at the O_2/C ratio of 0.60 is the main reason for its lower initial power density output and higher overall electrode polarization resistance compared to that of the bilayer structured SOFC operating at the similar O_2/C ratio.

The Ni-based SOFC is also operated at a significantly lower O_2/C ratio of 0.20 to investigate if the lower ratio would increase cell performance by preventing oxidation of the Ni. According to Fig. 6(a), the initial power density output of the Ni-based SOFC did not change much as the O_2/C ratio decreases from 0.60 to 0.20 at the constant cell voltage of 0.7 V. The XRD patterns from tested samples shown in Fig. 6(b) indicate no presence of the NiO phase, which suggests that the O_2/C ratio of 0.20 is low enough to stabilize the metallic phase during 10 h of cell operation. However, it also shows a very broad diffraction peak at $2\theta = 31^\circ$, which indicates the presence of carbon deposits at the low O_2/C ratio [23]. Due to this coking, the power density output of the Ni-based SOFC at the constant voltage of 0.7 V using the O_2/C ratio of 0.20 decreases to zero after operating it just for the 10 h. To summarize, the bilayer structured SOFC under the direct feed condition of the *n*-dodecane fuel mixtures significantly outperforms the conventional Ni-based SOFC in terms of both initial cell performance and coking resistance.

4. Conclusions

This work investigated the performance of liquid hydrocarbon fueled SOFCs using the Ni-based anode coupled with the MoO_2 microstructured-reformer layer. This novel anode design was found to show excellent power density output when *n*-dodecane is directly fed to the anode, and exhibits a significantly improved coking tolerance as compared to conventional Ni-based anode without the MoO_2 microstructured-reformer layer. The O_2/C ratio was found to have a significant influence on both the Ni-based anode and the microstructured MoO_2 reformer layers. At the O_2/C ratio of 0.64, the bilayer structured SOFC anode exhibits the maximum initial power density output of 4.3 W cm^{-2} at 0.6 V with neither the phase transformations of its active layers nor surface coke formation, which suggests that 0.64 is the optimum O_2/C ratio. Thus, this novel bilayer structured anode design with the MoO_2 microstructured-reformer layer shows great promise for the fabrication of efficient, economical and lighter SOFC systems that can be operated by directly feeding complex liquid fuels to the anode without the external reformers. If the MoO_2 microstructured- reformer layer is introduced as the filter into the Ni-based anode, we can

easily transform the conventional SOFC into the fuel flexible SOFC that can directly handle the various types of logistic fuels.

Acknowledgements

This work was supported financially by the National Science Foundation GOALI Program (Grant No. CBET-1034308), the Office of Naval Research (Grant No. N00014-12-1-0830) and Boeing Commercial Airplanes. This work was also supported by Ministry of Science, ICT and Future Planning (MSIP), and it was partially funded by USDA/NIFA through Hatch Project #WNP00807 titled: "Fundamental and Applied Chemical and Biological Catalysts to Minimize Climate Change, Create a Sustainable Energy Future, and Provide a Safer Food Supply"

Appendix A. Supplementary data

Supplementary data associated with this article can be found, in the online version, at http://dx.doi.org/10.1016/j.apcatb.2015.05.048

References

[1] S. Mclntosh, R.J. Gorte, Chem. Rev. 104 (2004) 4845–4865.
[2] W.Z. Zhu, S.C. Deevi, Mater. Sci. Eng. A 362 (2003) 228–239.
[3] M. Cimenti, J.M. Hill, Energies 2 (2009) 377–410.
[4] T. Hibino, A. Hashimoto, T. Inoue, J. Tokuno, S. Yoshida, M. Sano, Science 288 (2000) 2031.
[5] J.W. Fergus, R. Hui, X. Li, D.P. Wilkinson, J. Zhang, Solid Oxide Fuel Cells: Materials Properties and Performance, CRC Press Taylor & Francis Group, New York, 2009.
[6] C. Yang, Z. Yang, C. Jin, G. Xiao, F. Chen, M. Han, Adv. Mater. 24 (2012) 1439.
[7] H. Kishimoto, Y. Xiong, K. Yamaji, T. Horita, N. Sakai, M.E. Brito, H. Yokokawa, ECS Trans. 1 (2007) 1669.
[8] J.S. O'Brein, J.B. Giorgi, ECS Trans. 28 (2010) 221.
[9] K. Kendall, M. Slinn, J. Preece, J. Power Sources 157 (2006) 750–753.
[10] Z.F. Zhou, R. Kumar, S.T. Thakur, L.R. Rudnick, H. Schobert, S.N. Lvov, J. Power Sources 171 (2007) 856–860.
[11] J. Hoh, Y. Yoo, J. Park, H.C. Lim, Solid State Ionics 149 (2002) 157–166.
[12] Z. Zhan, S.A. Barnett, Science 308 (2005) 844–847.
[13] O. Marin-Flores, S. Ha, Appl. Catal. A: Gen. 352 (2009) 124–132.
[14] O. Marin-Flores, T. Turba, C. Ellefson, K. Wang, J. Breit, J. Ahn, M.G. Norton, S. Ha, Appl. Catal. B: Environ. 98 (2010) 186–192.
[15] O. Marin-Flores, T. Turba, C. Ellefson, J. Breit, M.G. Norton, S. Ha, Appl. Catal. A: Gen. 381 (2010) 18–25.
[16] O. Marin-Flores, T. Turba, C. Ellefson, L. Scudiero, J. Breit, M.G. Norton, S. Ha, Appl. Catal. B: Environ. 105 (2011) 61–68.
[17] V. Bhosle, A. Tiwari, J. Narayan, J. Appl. Phys. 97 (2005) 083539–083544.
[18] O. Marin-Flores, L. Scudiero, S. Ha, Surf. Sci. 603 (2009) 2327–2332.
[19] M. Bengisu, Engineering Ceramics, Springer, Heidelberg, New York, 2001, ISBN: 3-540-67687-2.
[20] G. Bae, J. Bae, P. Kim-Lohsoontorn, J. Jeong, Int. J. Hydrogen Energy 35 (2010) 12345–12358.
[21] C.A. Ellefson, O. Marin-Flores, S. Ha, M.G. Norton, J. Mater. Sci. 47 (2012) 2057–2071.
[22] B.W. Kwon, C. Ellefson, J. Breit, J. Kim, M.G. Norton, S. Ha, J. Power Sources 243 (2013) 203–210.
[23] E. Horváth, R. Puskás, R. Rémiás, M. Mohl, Á. Kukovecz, Z. Kónya, I. Kiricsi, Topics Catal. 52 (2009) 1242–1250.